Adsorption of α-Amylase in a Fixed Bed: Operating Efficiency and Kinetic Modeling

L. F. Bautista, M. Martínez, and J. Aracil
Dept. of Chemical Engineering, Universidad Complutense de Madrid, Ciudad Universitaria, 28040 Madrid, Spain

Kinetic studies on the adsorption of α-amylase from Aspergillus oryzae on the anion exchanger, Duolite A-568, and the hydrophobic resin, Duolite XAD-761, were carried out in a fixed bed. The efficiency with respect to the adsorbate and adsorbent was determined to estimate the performance of the process of adsorption. The effect of flow rate, α-amylase inlet concentration, temperature, and particle size of the packing was analyzed. In addition, the transient response, in the form of experimental breakthrough curves, was fitted using a phenomenological mathematical model accounting for the external-film and pore-diffusion mass-transfer mechanisms as well as axial dispersion along the column. Also, a Langmuir isotherm was included in the model to account for the extent of the equilibrium of adsorption. The model described satisfactorily the experimental breakthrough curves and it proved to predict successfully the behavior of a scaled-up bed using the kinetic and equilibrium parameters estimated previously. Thus, the mathematical model can be considered a reliable tool for process design and scale-up of similar systems.

Introduction

Usually, the purification of enzymes and other macromolecules, from a fermentation broth or from their natural sources, is carried out by empirical or semiempirical methods, after tedious and time-consuming experimental work.

The use of an adsorption step in industrial downstream processing requires stopping the adsorption stage before the saturation of the adsorbent is completed. The operating procedure just given is obviously performed to avoid losses of adsorbate in the effluent. At industrial scale, the time when the operation stops must be determined after an economic and, eventually, environmental evaluation, because not only the amount of solute adsorbed but the operating time has an important impact on the effective use of the column and on the final throughput of the process, too. The optimization of this and other operating conditions can be accomplished with the help of reliable mathematical models.

To date, different models have been used for basic studies at small scale. In the case of affinity chromatography, several mathematical models of increasing complexity have been reported, from the initial approaches with lumped kinetic mass-transfer parameters (Arnold et al., 1985; Chase, 1984) to more complete models accounting for the physicochemical mechanisms taking place along the process (Arve and Liapis, 1988; Sridhar, 1996; Niemeyer et al., 1996; Carta and Lewus, 2000).

Similar models have been applied to describe the experimental operation of adsorption of proteins in a fixed bed. Most of these studies have been carried out using some "model" proteins, such as bovine serum albumin (BSA), lysozyme, or human serum albumin (HSA). Usually, the adsorption interaction mechanism studied involved ion exchange (Skidmore et al., 1990; Johnston et al., 1991; Mao and Hearn, 1996; Sajonz et al., 1997; Yang et al., 1999). In spite of that, most of the studies about protein adsorption involving mathematical models were simulations or comparison between several theoretical models (Sridhar, 1996; Miyabe and Guiochon, 1999). Therefore, the application of phenomenological mathematical models to describe the kinetics of adsorption of large biomolecules on porous media in a fixed bed for industrial purposes is scarce. In addition, there is a lack of work to test those mathematical models against experimental systems that include different proteins and another type of mechanism such as adsorption by hydrophobic interactions, widely used in the separation and purification of industrial enzymes.

Correspondence concerning this article should be addressed to J. Aracil.

In the present work, the study of the effect of the operating variables on the process of adsorption of α-amylase from *Aspergillus oryzae* in a fixed bed was investigated. Furthermore, the kinetics was studied using a mathematical model that takes account of both external and internal mass-transfer resistances as well as of nonideal plug flow along the column. The application of the phenomenological model to the adsorption of an industrial enzyme in two different types of adsorbent will give the model a wider general validity.

Mathematical Model

The model used in the present work to fit the experimental data takes account of the effect of both intraparticle and external-film mass-transfer resistances. Simultaneously, instantaneous local adsorption equilibrium on the pore surface was considered. Furthermore, the following assumptions were made to set up the model equations:

(i) The system operates under isothermal conditions.

(ii) The equilibrium of adsorption is described by an isothermal equation in the form $q = f(c)$.

(iii) Intraparticle mass transport is due to Fickian diffusion, and it is characterized by the pore diffusion coefficient, D_p. Mass transfer across the boundary layer surrounding the solid particles is characterized by the external-film mass-transfer coefficient k_f.

(iv) The linear velocity of the liquid phase along the column, and the mass-transfer parameters are independent of the solute concentration in the bulk liquid phase.

(v) Axial dispersion is considered to account for nonideal flux along the longitudinal axis of the column.

(vi) The macroporous adsorbent particles are spherical and homogeneous in size and density.

Based on the preceding assumptions, the mass balance within a differential radial section of an adsorbent bead can be expressed as

$$\frac{\partial c}{\partial t} + \left(\frac{1-\epsilon_p}{\epsilon_p}\right)\rho\frac{\partial q}{\partial t} = D_p\left(\frac{\partial^2 c}{\partial r^2} + \frac{2}{r}\frac{\partial c}{\partial r}\right) \tag{1}$$

Assuming instantaneous equilibrium

$$\frac{\partial q}{\partial t} = \frac{\partial c}{\partial t}\frac{dq}{dc} \tag{2}$$

Then, rearranging Eq. 1

$$\frac{\partial c}{\partial t} = \frac{1}{\left[1+\rho\left(\frac{1-\epsilon_p}{\epsilon_p}\right)\frac{dq}{dc}\right]} D_p\left(\frac{\partial^2 c}{\partial r^2} + \frac{2}{r}\frac{\partial c}{\partial r}\right) \tag{3}$$

The mass balance in a cross section of the column yields

$$-D_L\frac{\partial^2 C}{\partial z^2} + v\frac{\partial C}{\partial z} + \frac{\partial C}{\partial t} + \left(\frac{1-\epsilon}{\epsilon}\right)\frac{3k_f}{R}(C - c|_{r=R}) = 0 \tag{4}$$

The symmetry condition at the center of the particles is expressed as

$$\left.\frac{\partial c}{\partial r}\right|_{r=0} = 0 \tag{5}$$

The continuity condition on the external surface of the adsorbent beads is as follows

$$-D_p\epsilon_p\left.\frac{\partial c}{\partial r}\right|_{r=R} = k_f(C - c|_{r=R}) \tag{6}$$

The contour conditions at both ends of the column are given by the following equations (Danckwerts, 1953)

$$-D_L\left.\frac{\partial C}{\partial z}\right|_{z=0} = v(C_0 - C|_{z=0}) \tag{7}$$

$$\left.\frac{\partial C}{\partial z}\right|_{z=L} = 0 \tag{8}$$

Finally, the following initial conditions are considered

$$\begin{array}{llll} C = 0 & 0 \le z \le L & (t \le 0) \\ C = C_0 & 0 = z & (t > 0) \\ c = 0 & 0 \le z \le L & (t \le 0) \\ q = 0 & 0 \le z \le L & (t \le 0) \end{array} \tag{9}$$

Since nonlinear adsorption equilibrium was considered, the preceding set of partial differential equations was solved numerically by a reduction to a set of ordinary differential equations using the orthogonal collocation method (Villadsen and Stewart, 1967; Carey and Finlayson, 1975). The solution of this set of coupled equations was performed by a mathematical algorithm, developed in Fortran, implemented into a computer program. The program used the subroutine D02EAF from the NAG Fortran Library (Numerical Algorithms Group Inc., Downers Grove, IL) that applies the variable-order, variable-step Gear method (Gear, 1971).

The values of D_p and k_f were obtained by fitting the mathematical model to the experimental breakthrough curves and further optimization using the Simplex method. The objective function was expressed as

$$\Phi = \sum_{i=1}^{N}\left[(C_i^{\exp} - C_i)^2\right] \tag{10}$$

The parameter optimization stopped when the following condition was fulfilled

$$\sqrt{\frac{\sum_{j=1}^{M}\left[(\Phi_j - \Phi_m)^2\right]}{M+1}} \le 10^{-10} \tag{11}$$

Table 1. Characterization of the Adsorbents

	Duolite XAD-761	Duolite A-568
Specific gravity (g/cm^3)*	1.08	0.94
Pore volume (cm^3/g)**	0.42	0.53
Skeletal density (g/cm^3)**	1.97	1.89
Porosity**	0.45	0.50
Average pore size (nm)**	22.5	27.3
BET surface area (m^2/g)†	27.2	92.8
Swelling (% vol)*	7	7

*From Duolite XAD-761 and Duolite-568 Technical Sheets, Rohm and Haas Co.
**Measured by mercury porosimetry.
†Measured by nitrogen adsorption.

Experimental Studies

Materials

α-Amylase (α-1,4-glucan-4-glucanohydrolase, EC 3.2.2.1) from *A. oryzae* was obtained by purification of the commercial Fungamyl 1600 BG, kindly supplied by Novo Nordisk Bioindustrial S.A. (Madrid, Spain). The purification protocol consisted of a fractionated precipitation, followed by recrystallization in acetone (Akabori et al., 1954).

The weak anion exchanger, Duolite A-568, and the hydrophobic adsorbent, Duolite XAD-761, were a gift from Rohm and Haas España S.A. (Barcelona, Spain). The physical properties are listed in Table 1. Three fractions of different particle size (0.20–0.32, 0.32–0.50, and 0.50–0.80 mm) in the range of that commonly used for industrial applications were employed in the present study for every adsorbent used. The pretreatment applied to both resins has been previously reported (Bautista et al., 1999).

Mobile phases used for the adsorption of α-amylase on Duolite XAD-761 and Duolite A-568 were 0.05-M phosphate buffer (pH 6.0, ionic strength 0.35 M) and 0.05 M tris/HCl buffer (pH 7.0, ionic strength 0.60 M), respectively. Further, 0.04 M $CaCl_2$ was added to every buffer solution to maintain the enzymatic activity and the structural stability of the a-amylase molecules (Vallee et al., 1959; Janecek and Baláž, 1992). Finally, the ionic strength was adjusted by addition of the adequate amounts of NaCl.

The chemicals used for buffer preparation were analytical grade. All buffer solutions were filtered through 0.80 μm of cellulose ester membranes (AAWP 047 00, Millipore, Bedford, MA) prior to use.

Equipment

Fixed-bed experiments were performed in an FPLC System (Pharmacia LKB, Uppsala, Sweden), adapted to the research experiments, and arranged as sketched in Figure 1. The system consisted of a Moduline-jacketed glass column (Amicon Corp., Danvers, MA) with a 10- or 16-mm ID, packed with the selected amount of the corresponding resin. The adsorption solution containing the α-amylase and the desorption buffer were fed to the column through the two P-500 piston pumps. The concentration of adsorbate and the pH in the effluent were continuously monitored using, respectively, an UV-M-II spectrophotometer and a pH monitor fitted with their corresponding flow cells. A column bypass was provided so that calibration of the feed solution and initial base-line settings could be obtained by the ultraviolet absorbance at 280 nm. The system was equipped with two PSV-50 solenoid-switching valves and an MV-7 injection valve to select the flow path along the equipment. All of the devices described were fully controlled by the FPLC-Director software implemented in a personal computer through the interface controller module LCC-500 CI. A thermostatic bath with external circulation (Heto DT1 CB-8-30e, Heto-Holten, Allerød, Denmark) was used to keep the column at the operating temperature during the development of each experiment.

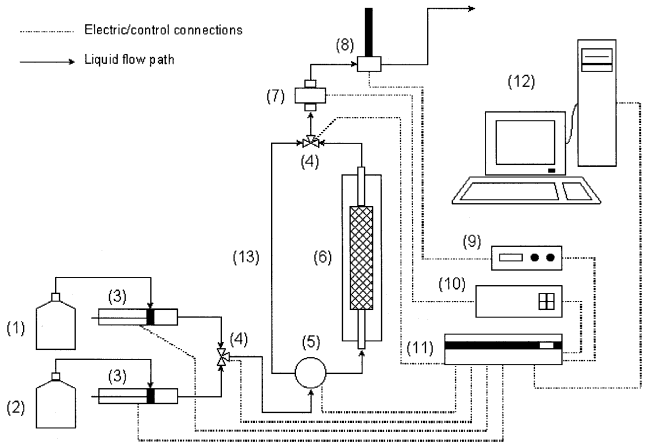

Figure 1. The fixed-bed apparatus.

(1) Adsorption solution reservoir, (2) desorption buffer reservoir, (3) P-500 piston pumps, (4) 3-ways solenoid valves, (5) 7-ways injection valve, (6) jacketed glass column, (7) UV flow cell, (8) pH flow cell, (9) pH monitor, (10) UV monitor, (11) LCC-500 CI controller, (12) personal computer, (13) column bypass.

Procedures

The column packed with the appropriate amount of adsorbent and fitted into the FPLC system was conditioned overnight with the mobile phase at the selected temperature and flow rate. A typical experiment was operated in the following manner: the column bypass was selected to obtain control values and base lines of the adsorption α-amylase solution and the corresponding buffer solution, respectively. The adsorption stage started by switching the bypass back to feeding the column with the adsorbate solution. When the saturation of the bed was achieved, the 3-way solenoid valve switched and the desorption stage commenced when the buffer was pumped through the column until the base line was attained again. The enzyme concentration in the outlet stream was continuously monitored by measuring the ultraviolet absorbance at 280 nm using the experimental calibration curve.

Results and Discussion

The adsorption equilibrium of α-amylase from *A. oryzae* on Duolite XAD-761 and Duolite A-568 was previously studied (Bautista et al., 1999). The results showed that the equilibrium was favorable and nonlinear, and it was adequately described by a Langmuir isotherm (Eq. 12) within the tem-

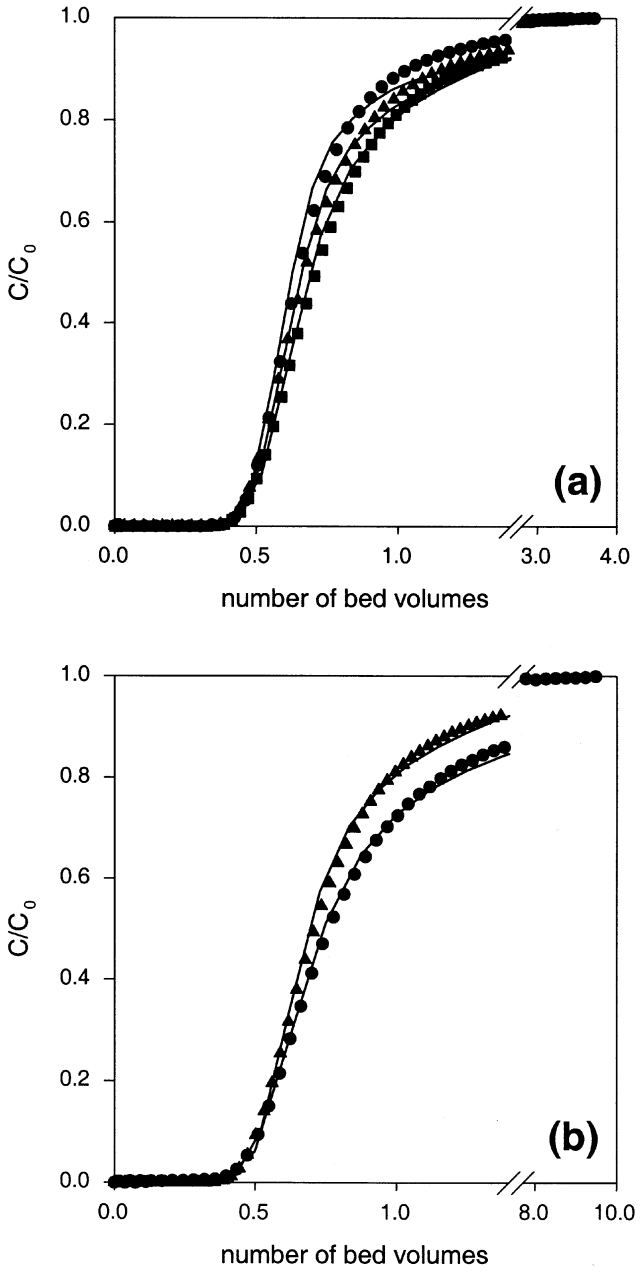

Figure 2. Experimental (dots) and model (solid lines) breakthrough curves of α-amylase on Duolite XAD-761 at 20°C.

(a) Effect of flow rate for $C_0 = 2.5$ mg/mL (■ 0.25 mL/min, ▲ 0.50 mL/min, ● 1.00 mL/min), and (b) effect of inlet adsorbate concentration at a flow rate of 0.25 mL/min (● 0.50 mg/mL, ▲ 2.50 mg/mL).

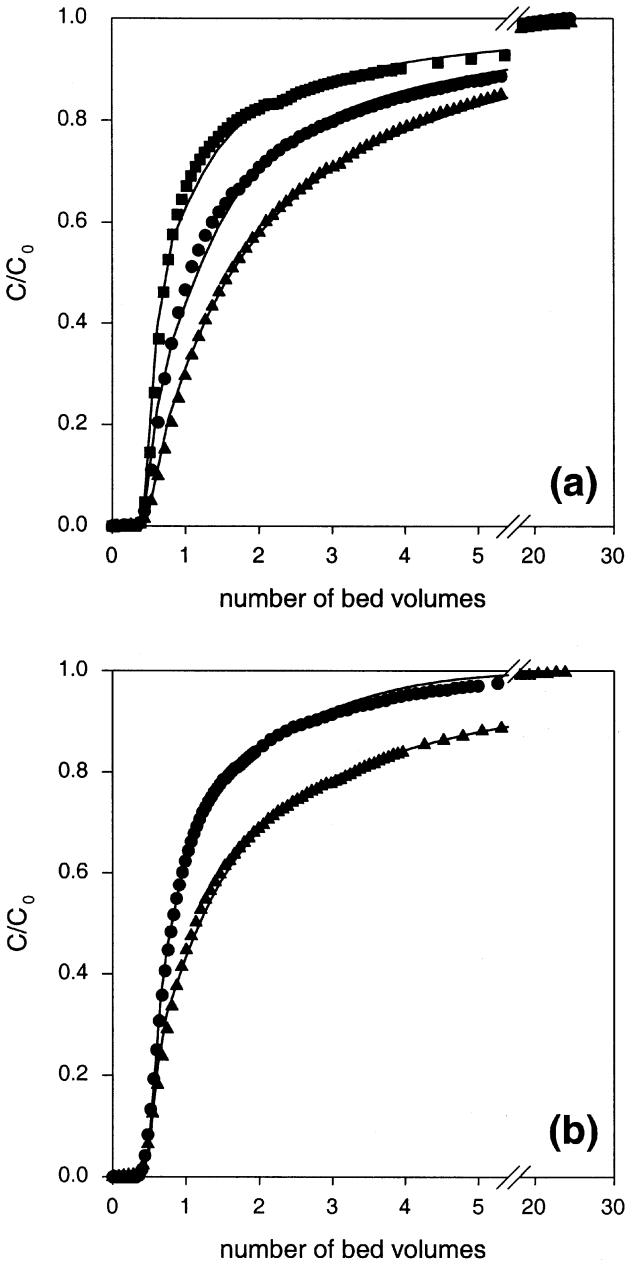

Figure 3. Experimental (dots) and model (solid lines) breakthrough curves of α-amylase on Duolite A-568 at 25°C.

(a) Effect of flow rate for $C_0 = 1.0$ mg/mL (■ 0.25 mL/min, ▲ 0.50 mL/min, ● 1.00 mL/min), and (b) effect of inlet adsorbate concentration at a flow rate of 0.25 mL/min (■ 0.50 mg/mL, ▲ 2.50 mg/mL).

perature and concentration range reported

$$q = \frac{Q_m \cdot b \cdot c}{1 + b \cdot c} \tag{12}$$

Figures 2 and 3 show some of the experimental breakthrough curves obtained at different operating conditions for the hydrophobic resin and the anion exchanger, respectively. In both systems, one gram of adsorbent of the selected particle-size range was packed in a 10-mm-ID column, yielding length columns of 31 and 25 mm for the anion exchange and hydrophobic bed, respectively.

In all the experiments, asymmetric breakthrough curves were observed due to a slow asymptotic approach to the bed saturation when dimensionless concentration was higher than 0.90. This must be caused by a hindered diffusion process within the pores at high adsorption surface coverage, because

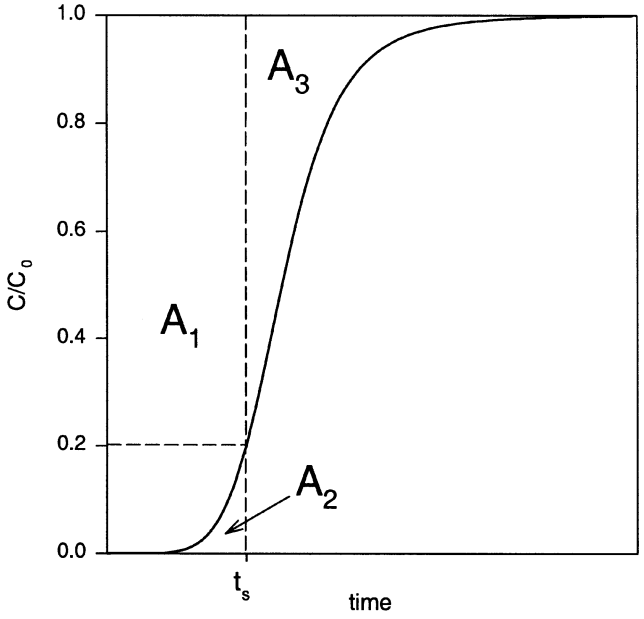

Figure 4. A general breakthrough curve for the geometric interpretation of the efficiencies.

A_1: area above the curve from $t = 0$ to $t = t_s$. A_2: area below the curve from $t = 0$ to $t = t_s$. A_3: area above the curve from $t = t_s$ to $t = \infty$.

of the relatively low ratio between the mean pore diameter of the adsorbent and the size of the α-amylase molecule that resembles an ellipsoid of dimensions $8.0 \times 4.5 \times 3.5$ nm (Boel et al., 1990; Swift et al., 1991).

The study of the fixed-bed operation must include an estimation of the efficient use of both adsorbate and adsorbent. Figure 4 shows the geometric interpretation of the utilization of adsorbate and adsorbent based on the areas of the different zones of a typical breakthrough curve. In order to quantify the performance of the adsorption operation in a fixed bed, several effectiveness factors have been defined in the literature. Effectiveness factors with respect of adsorbate, e_S, and adsorbent, e_R, can be expressed, respectively, as follows (Sridhar et al., 1994; Niemeyer et al., 1996)

$$e_S = \frac{A_1}{A_1 + A_2} \tag{13}$$

$$e_R = \frac{A_1}{A_1 + A_3} \tag{14}$$

However, from the results of the present work (Figures 2 and 3), it can be noticed that the breakthrough curves are significantly asymmetric with respect to the inflection point. The complete saturation of the resin was slowly achieved when the column loading was high. Thus, the numerical estimation of A_3 was liable to numerical integration errors, yielding values of e_R that are often difficult to correlate with the effect of the operating variables studied. Moreover, when the work is performed in large-scale columns, or due to the operating conditions the saturation takes longer, the estimation of the bed efficiency according to Eq. 14 may be highly time-consuming as well as a very expensive waste of mobile phase and often very valuable adsorbate. To overcome this problem, the effectiveness factor with respect of the adsorbent was numerically estimated according to the following equation

$$e'_R = A_1 \frac{U \cdot C_0}{(q_0 \cdot W + \epsilon_L \cdot V \cdot C_0)} \tag{15}$$

From the preceding equation, the ratio of the actual amount of adsorbate inside the column ($A_1 \cdot U \cdot C_0$) to the maximum amount of adsorbate inside the column (adsorbed, $q_0 \cdot W$, plus contained within the bulk liquid phase between particles, $\epsilon_L \cdot V \cdot C_0$) can be calculated. So, factor e'_R allows the comparison of the bed efficiency, relative to the corresponding equilibrium capacity, at different experimental operating conditions in any adsorbent/adsorbate system.

In the present work, the effectiveness parameters e'_R and e_S were calculated for a 20% cutoff, that is, for a t_s value corresponding to an enzyme concentration in the mobile phase leaving the column equal to 20% of the enzyme concentration in the inlet stream. This cutoff value was chosen arbitrarily in order to compare the results between different experiments carried out at different operating conditions.

In these conditions, the calculations yielded very high levels of e_S in all the experiments, with all the values in the range 0.95–0.97. These high values of e_S were due to the steep curve following the breakthrough of the bed that resulted in low values of the area A_2.

Effect of inlet concentration

In both resins, e'_R increased as the inlet adsorbate concentration increased (Figure 5). For larger feed concentration experiments, steeper breakthrough curves were obtained (Figures 2b and 3b) because of the lower mass-transfer flux from the bulk solution to the particle surface due to the weaker driving force achieved (Eq. 6). In addition, at high concentration, the isotherm gradient (Eq. 3) was lower, yielding a higher driving force along the pores. Thus, the equilibrium was attained faster for those experiments carried out at higher α-amylase concentration. This was clearly observed in Figures 5a and 5b, since the e'_R linearly increased with C_0. From mass-balance calculations, the increase in the inlet α-amylase concentration from 0.5 mg/mL to 2.5 mg/mL also resulted in a fivefold increase in the throughput of each adsorption step when a 20% cutoff was assumed.

Effect of flow rate

The flow rate and, thus, the linear velocity of the fluid phase affects the thickness of the boundary layer surrounding the particles and the external mass-transfer coefficient that is a function of the latter. Within the experimental range, the effect of flow rate on the bed efficiency was negligible for the adsorption of α-amylase on Duolite XAD-761 (Figure 6a). Only a slight increase in e'_R at low velocity was measured for the adsorption on Duolite A-568 (Figure 6b). That indicates that the external-film mass-transfer resistance makes a slight contribution to the kinetic control on the overall mass-transfer mechanism. However, until the concentration in the efflu-

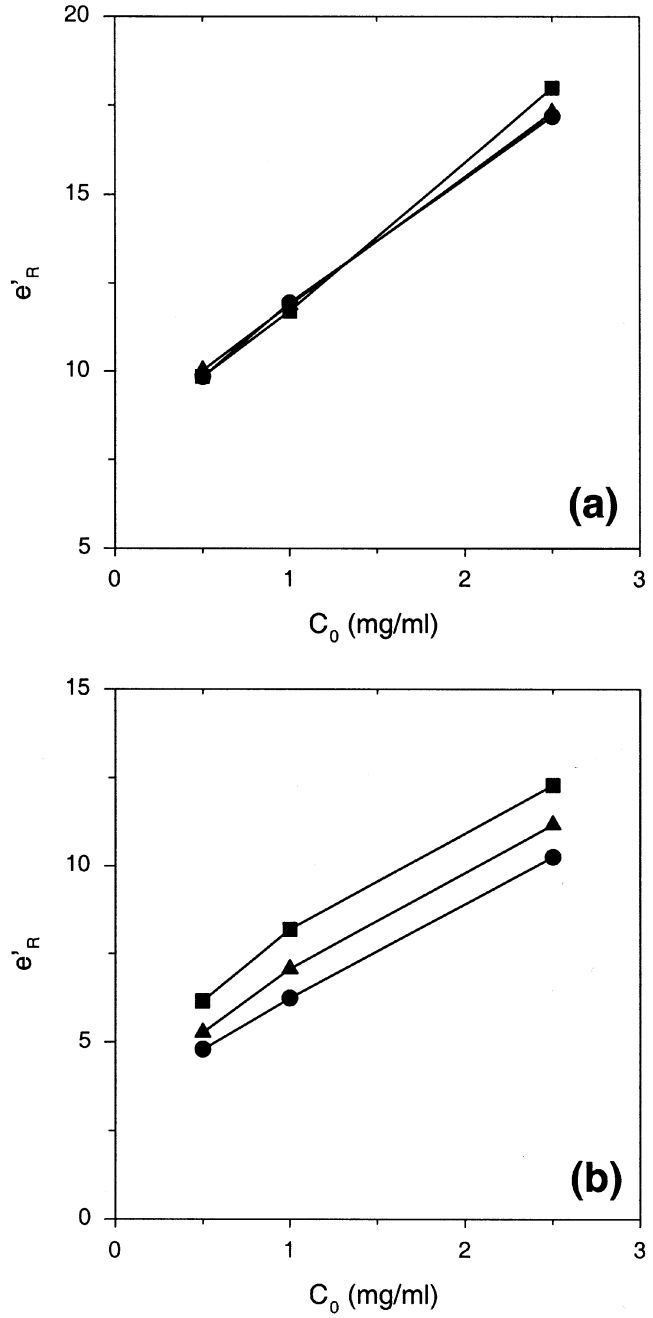

Figure 5. Effect of C_0 on e'_R for the adsorption of α-amylase on (a) Duolite XAD-761, and (b) Duolite A-568 at a time corresponding to a 20% of the breakthrough [$C(t = t_s, z = L)/C_0 = 0.2$] at different inlet adsorbate concentrations (■ 0.25 mL/min, ▲ 0.50 mL/min, ● 1.00 mL/min).

ent was 20% of the inlet feed concentration, the throughput of the adsorption step linearly increased with the flow rate. Although the preceding feature is interesting from the industrial point of view, the increase in the flow rate must be balanced against the rise in the operating cost due to the larger pressure drop and pumping costs.

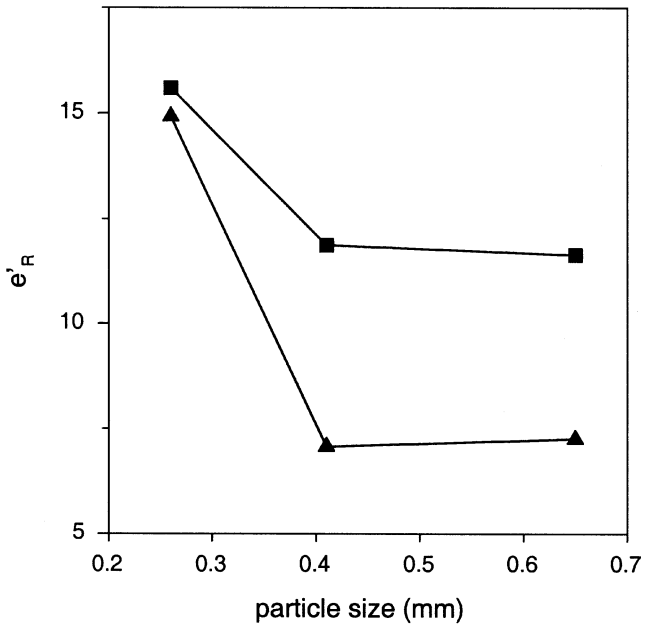

Figure 6. Effect of particle size on e'_R for the adsorption of α-amylase on (■) Duolite XAD-761 and (▲) Duolite A-568 at a time corresponding to a 20% of the breakthrough [$C(t = t_s, z = L)/C_0 = 0.2$].

Effect of particle size

The experiments showed that the e'_R was approximately constant for both resins when the average particle size was larger than 0.41 mm, increasing for smaller particles (Figure 6). As the diameter of the beads increases, the thickness of the stagnant film around the particles also increases, as does the total length of the path inside the pores. Since the effect of flow rate was studied using an average particle size of 0.41 mm, and only a slight or even negligible external mass-transfer resistance was observed, the increase in the effectiveness for smaller particles must be mainly due to a decrease in the internal diffusion control. Under these conditions, the overall kinetics of the process was faster because the time for a molecule of adsorbate to reach the adsorption site was shorter, since the diffusional path along the pores was shorter, too. The negative effect of the particle size on the mass-transfer flux from the interstitial α-amylase solution to the external surface of the adsorbent particles was qualitatively analogous, and was related to the positive effect of the flow rate, as mentioned in the preceding section. The quantitative influence of both parameters on the external-film mass-transfer coefficient is given by different correlations reported in the literature (Carberry, 1960; Hougen, 1961; Hsiung and Thodos, 1977; Hidajat et al., 1995), whose validity depends on specific Reynolds number ranges.

Effect of temperature

The equilibrium of adsorption of α-amylase on Duolite XAD-761 is slightly exothermic (Bautista et al., 2000). Thus, an increase in the operating temperature yielded lower values of the maximum capacity of the resin, Q_m, and larger

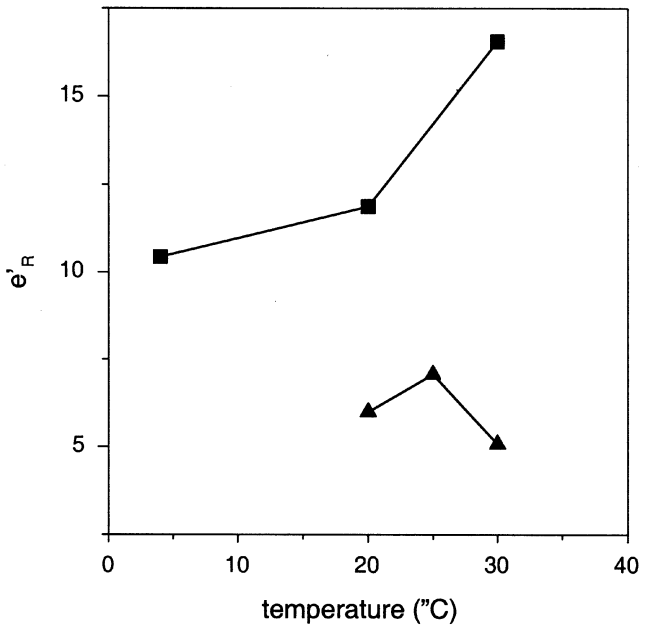

Figure 7. Effect of temperature on e'_R for the adsorption of α-amylase on (■) Duolite XAD-761 and (▲) Duolite A-568 at a time corresponding to a 20% of the breakthrough [$C(t = t_s, z = L)/C_0 = 0.2$].

overall mass fluxes by diffusion. Then, the bed saturation was achieved faster and the e'_R increased significantly (Figure 7).

The behavior of the anion exchange system, α-amylase/Duolite A-568, was different and not so straightforward. Here, the effect of Q_m and diffusivities were concurrent and the value of the saturation capacity increased with temperature as well as the mass-transfer rates. So, although the adsorbate molecules diffused faster, more α-amylase was required to attain the maximum capacity of the resin. As a result, the value of e'_R slightly increased as temperature increased from 20°C to 25°C and decreased as temperature increased from 25°C to 30°C, even though these changes were less significant than those observed for the hydrophobic adsorbent.

Modeling

The mathematical model describing the kinetics of the adsorption process was used to fit the experimental breakthrough curves in order to determine the mass-transfer parameters, that is, the effective pore-diffusion and the external-film mass-transfer coefficients, by minimization of the objective function (Eq. 10), as previously described. The best fitting values of the parameters for both resins are shown in Table 2.

The effective pore-diffusion coefficient increased with temperature for both the hydrophobic and the anion-exchange adsorption systems. The ratio between D_p and the molecular diffusivity, estimated through the Polson equation (Polson, 1950), was approximately constant over the temperature range studied for the adsorption of α-amylase on Duolite A-568 (Table 3). The same feature was observed at 20 and 30°C for the hydrophobic resin; however, at 4°C, the ratio D_m/D_p was found to be significantly lower than expected if the same pore-diffusion mechanism was the main contributor to mass transfer inside the pores. This was also observed during batch experiments and explained on the basis of a shift in the contribution mechanism to internal mass transfer besides pore diffusion at decreasing temperature (Bautista et al., 2000).

The effect of the flow rate on the adsorption process is characterized by the external-film mass-transfer coefficient. Within the experimental range, the external diffusion was also a mass-transfer control mechanism. The optimization of the objective function, Φ, was sensitive to changes, both in k_f (expressed in the form of the Sherwood number) and in D_p in the proximity to their optimum values (Figure 8). The values of k_f determined through the optimization of the breakthrough curves agreed with those predicted by the correlation reported by Hidajat et al. (1995) that is suitable at low Reynolds numbers within the 0.01−0.04 range.

Table 2. Optimum Model Parameters Obtained from Experiments Carried Out at Different Operating Conditions

	T (°C)	C_0 (g/L)	Flow rate (mL/min)	$D_p \cdot 10^{11}$ (m^2/s)	$k_f \cdot 10^6$ (m/s)
Duolite XAD-761	20	0.5	0.25	1.3	5.4
			0.50	1.6	8.9
			1.00	1.5	13.0
		1.0	0.25	1.7	2.7
			0.50	1.8	9.0
			1.00	1.7	17.0
		2.5	0.25	1.8	2.8
			0.50	1.7	8.1
			1.00	2.0	18.0
	4	1.00	0.50	1.5	7.1
	30	1.00	0.50	2.4	9.2
Duolite A-568	25	0.5	0.25	2.0	1.0
			0.50	2.3	3.1
			1.00	2.1	5.1
		1.0	0.25	2.5	1.5
			0.50	2.6	2.3
			1.00	2.5	2.5
		2.5	0.25	2.3	0.6
			0.50	2.6	1.7
			1.00	2.5	4.1
	20	0.50	0.50	2.0	1.3
	30	0.50	0.50	2.8	4.5

Table 3. Pore-Diffusion Coefficient Estimated as the Average of the Optimum Fitted Values at Each Temperature

	T (°C)	D_p (m^2/s)	D_m/D_p
Duolite XAD-761	4	$1.5 \cdot 10^{-11}$	3.0
	20	$1.7 \cdot 10^{-11}$	4.3
	30	$2.4 \cdot 10^{-11}$	4.0
Duolite A-568	20	$2.0 \cdot 10^{-11}$	3.7
	25	$2.4 \cdot 10^{-11}$	3.5
	30	$2.8 \cdot 10^{-11}$	3.4

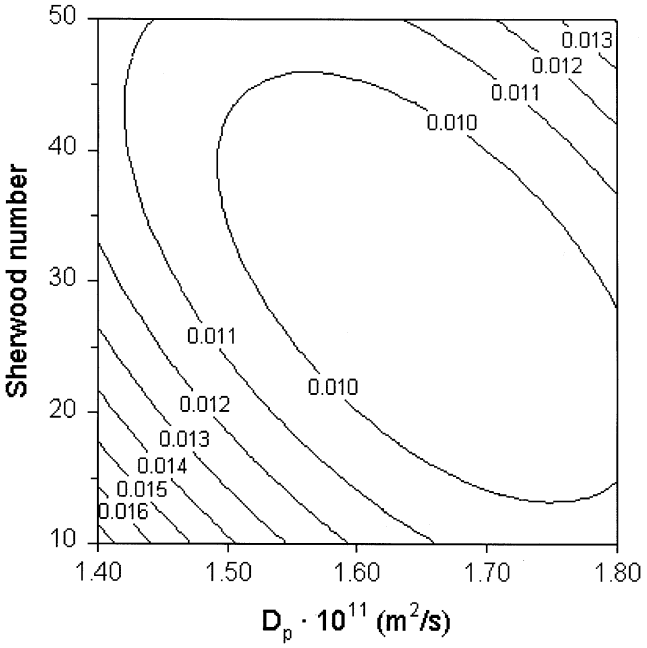

Figure 8. Example of a contour plot of the objective function (Φ) for the simultaneous optimization of D_p and k_f.

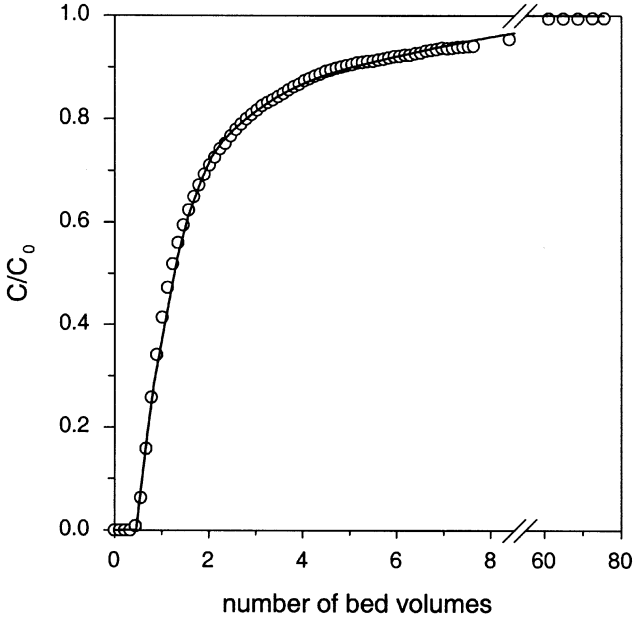

Figure 9. Scale-up of α-amylase on Duolite A-568 showing the experimental (○) and simulated (——) breakthrough curve.

Scale-Up, Validation and Simulation

Due to the nature of a phenomenological model accounting for the physicochemical steps describing the adsorption-diffusion mechanism, the model parameters obtained in the previous section should adequately predict the behavior of the process beyond the experimental system and bed features, where D_p, k_f, and the adsorption isotherm were determined. So, the mathematical model and the model parameters were validated using a column of different length-to-diameter ratio than that used in the former modeling experiments.

As an example, Table 4 shows the average value of the pore-diffusion coefficient at the operating temperature used in the simulation, the isotherm parameters previously estimated, and the experimental operating conditions of the validation experiments. Figure 9 shows good agreement between the experimental breakthrough curve and that predicted by the model, indicating the applicability of the pore-diffusion model described earlier to the design, scale-up, and simulation of the adsorption of α-amylase on the systems under study.

Table 4. Operating Conditions and Model Parameters Used in the Scale-Up

Bed length (cm)	16.3
Bed diameter (cm)	1.6
R (mm)	0.41
ϵ	0.58
C_0 (mg/mL)	2.50
Flow rate (mL/min)	5.0
T (°C)	25.0
D_p (m^2/s)	$2.4 \cdot 10^{-11}$
k_f (m/s)	$8.2 \cdot 10^{-6}$
Q_m (mg/g)	45.4
b (mL/mg)	0.84

Concerning the design and scale-up of the process, it is of great interest to know the effect of the key parameters and variables affecting the adsorption process. Thus, the mathematical model was employed to simulate the adsorption of a-amylase on a Duolite A-568 column using an inlet concentration of 2.5 mg/mL. Figure 10 shows the concentration profile of α-amylase along the longitudinal axis of the column at different operating times. It was observed that the profile gradually approached a more symmetric shape, suggesting a constant-pattern behavior. For a more accurate discussion, the length of the breakthrough front as a function of time was determined using the curves just given and plotted in the inset of Figure 10. Here, the constant pattern behavior was clearly shown, since the concentration profile was fully developed and so the length of the breakthrough front (Wankat, 1994) that reached a constant value of about 175 cm within the 150–200 minute range. This is of great importance for the design of an adsorption column in order to enable the process to operate with the highest possible efficiency, allowing optimizing the throughput of the industrial process.

So, for the following simulations, in the same operating conditions as earlier, a bed length of 400 cm was selected to ensure a process capable to achieve high efficiencies within the range of the common operating conditions found in these systems.

Figure 11 shows the effect of the pore-diffusion coefficient. As D_p decreased, the breakthrough point was attained sooner and lower steep curves were obtained with the consequent decrease in both e_S and e'_R. For sufficiently low values of D_p, the sigmoidal shape of the breakthrough curves lose their symmetry with respect to the inflection point, drastically decreasing the efficiencies due to a severe internal mass-transfer control that does not allow the full development of the

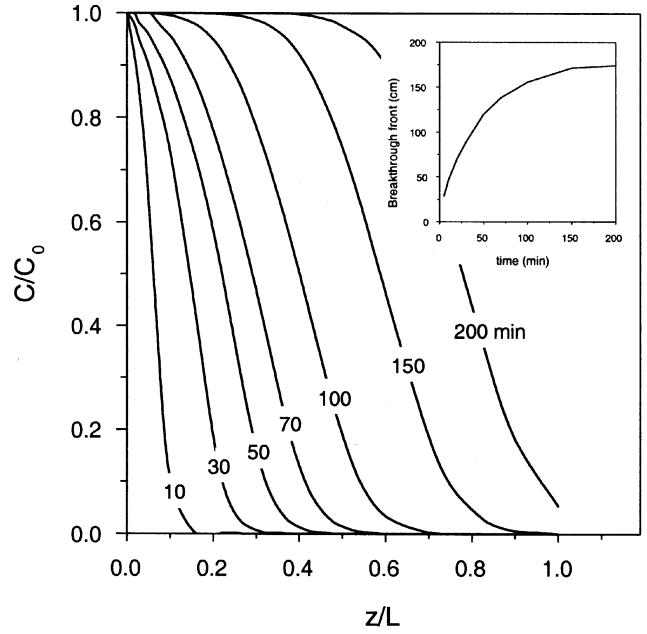

Figure 10. Simulated axial concentration profile of α-amylase at different times in a column (16 mm ID $\times$ 400 cm) packed with Duolite A-568.

The inset plot shows the change in the length of the breakthrough front with time. (Data used in the simulation: T = 25°C, C_0 = 2.5 mg/mL; flow rate: 5.0 mL/min, $D_p = 2.4 \cdot 10^{-11}$ m^2/s).

concentration profile along the column. For large molecules such as proteins, the molecular diffusivity proportionally increases as $M_w^{-1/3}$ (Polson, 1950), ranging from $D_m \sim 10^{-10}$ m^2/s, for small polypeptides, to $D_m \sim 3 \cdot 10^{-12}$ m^2/s, for large globular proteins.

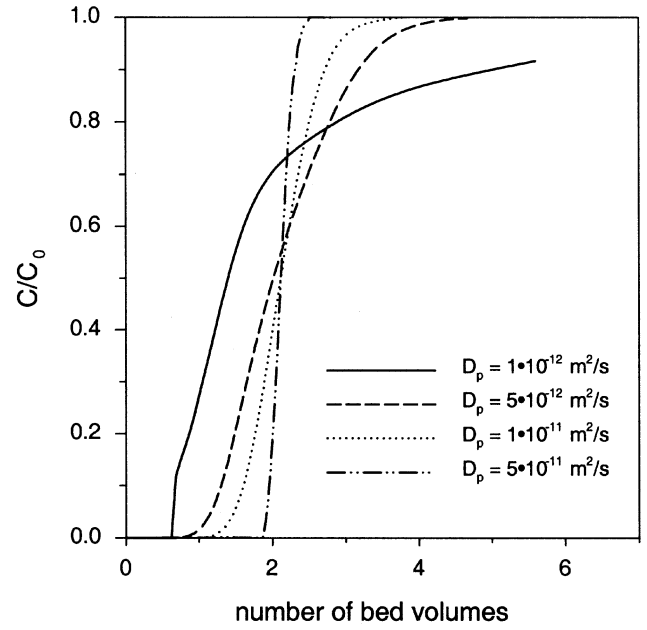

Figure 11. Simulation of the effect of the pore-diffusion coefficient.

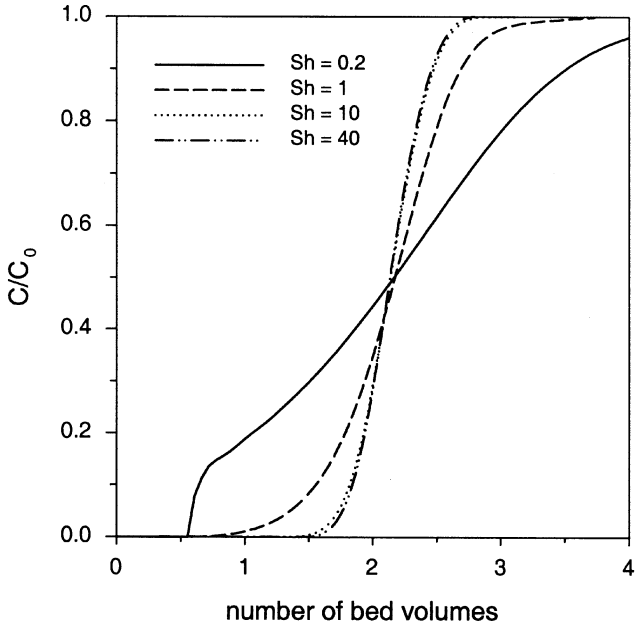

Figure 12. Simulation of the effect of the Sherwood number.

For a specific diffusing protein in a specific packed-bed system, the variation of the Sherwood number is directly caused by variations in the external-film mass-transfer coefficient. The slope of the breakthrough curves become larger (Figure 12) as Sh increases by decreasing the mass-transfer limitations suffered by the molecules of solute crossing the liquid external film surrounding each adsorbent particle. For higher Sh values, the breakthrough curves tend to be coincidental when the external diffusion does not exert any mass-transfer control in the kinetics of the overall process. On the other end, a severe external mass-transfer control was obtained for very low values of Sh that produced nonsigmoidal curves yielding very poor effectiveness factors for the adsorption process. In these cases, the sudden and steep breakthrough takes place for a number of bed volumes approaching the void-volume value of the fixed bed.

The effect of feed concentration is plotted in Figure 13. Because an initial α-amylase concentration lay in the saturation plateau of the isotherm, the column is operating with high efficiency, corresponding to very steep breakthrough curves. However, as C_0 decreases, the breakthrough of the bed occurs at the same number of bed volumes, but the slope decreases, yielding low effectiveness factors, because the mass-transfer driving forces for both the external and internal diffusion mechanisms greatly decrease.

The simulation shows that the effect of particle radius (Figure 14) follows a typical pattern, with better performance for smaller particles. The design and scale-up of an industrial process obviously need an optimization with the consequent increase in pressure drop and pumping costs.

Conclusions

The adsorption of α-amylase from *A. oryzae* on a hydrophobic resin and on an anion exchanger in a fixed bed have been studied.

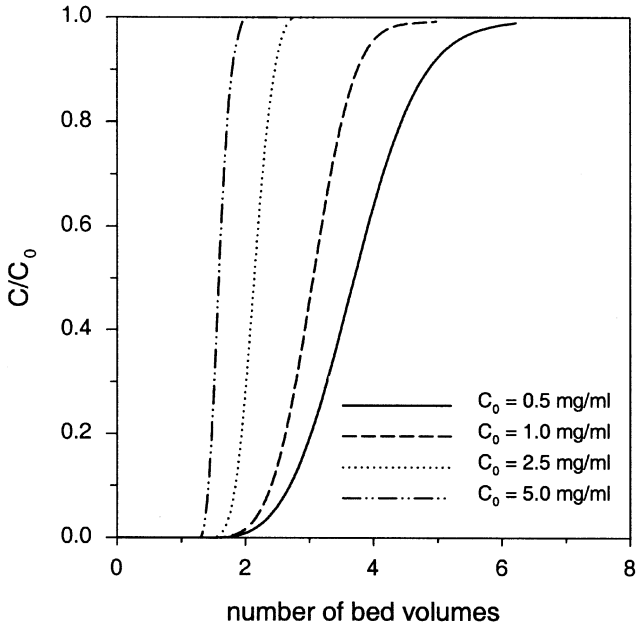

Figure 13. Simulation of the effect of the inlet concentration.

The effectiveness factor with respect of the adsorbent (e'_R) was used to quantify the performance of the process at different operating conditions. The efficiency increased with the inlet α-amylase concentration in both adsorbents, mainly due to the increasing concentration gradient within the pores of the adsorbent particles. The e'_R was approximately constant in the experimental flow-rate range studied, because the external mass transfer was not the controlling mechanism of the process, although the throughput increased with the linear velocity. The temperature favored the effectiveness of the bed for the hydrophobic resin, although the amount adsorbed decreased in these conditions due to the equilibrium constrains. However, the effect of temperature on the e'_R of the anion exchange system was more complex due to the balance of the opposite contributions of the equilibrium capacity of the adsorbent and the mass-transfer resistances.

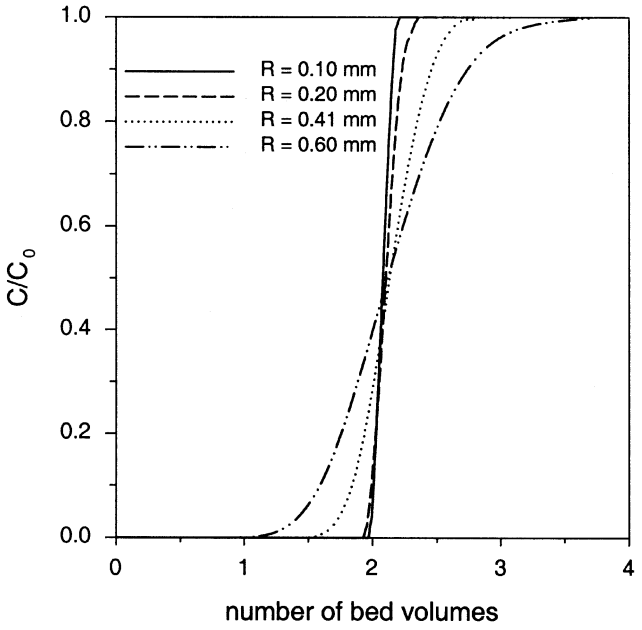

Figure 14. Simulation of the effect of the particle radius.

Furthermore, a mathematical model accounting for external-film and pore-diffusion mass-transfer mechanisms, axial dispersion, and nonlinear isotherm was used to fit the experimental breakthrough curves. The model reproduced adequately the experimental results once the best-fitting parameters were attained. The shape of the breakthrough curves was sensitive to changes in both the pore diffusion coefficient and the external-film mass-transfer coefficient. This showed the control of both mass-transfer mechanisms.

The model simulation proved the feasibility of successfully predicting the behavior of a larger bed with a different length-to-diameter ratio. Thus, the model is a useful and reliable tool for the design and scale-up for the adsorption of other biomolecules where a similar diffusion mechanism takes place.

Acknowledgment

Financial support from the Commission of the European Communities (project BE-8138, Brite-EuRam II Programme) is gratefully acknowledged.

Notation

b = parameter in Langmuir isotherm
c = solute concentration in the liquid phase inside the pores
C = solute concentration in the bulk liquid phase
C_0 = initial solute concentration in the bulk liquid phase
D_L = axial dispersion coefficient
D_m = molecular diffusivity
D_p = pore diffusion coefficient
k_f = external-film mass-transfer coefficient
L = length of the fixed bed
N = number of experimental values used in the estimation of Φ
M = number of optimization parameters
M_w = molecular weight
q = solute concentration on the adsorbed phase
Q_m = maximum adsorption capacity of the resin
q_0 = solute concentration on the adsorbed phase in equilibrium with a concentration C_0 in the liquid phase
R = average particle radius
Sh = Sherwood number ($2Rk_f/D_m$)
U = flow rate
v = interstitial fluid velocity along the column

Greek letters

ϵ = bed voidage
ϵ_p = particle porosity
Φ = objective function for optimization (Eq. 9) at each vertex of the Simplex triangle
Φ_m = average value of Φ at each Simplex triangle
ρ = skeletal particle density

Literature Cited

Akabori, S., T. Ikenaka, and B. Hagihara, "Isolation of Crystalline Taka-Amylase A from Takadiastase Sankyo," *J. Biochem.*, **41**(5), 577 (1954).

Arnold, F. H., H. W. Blanch, and C. R. Wilke, "Analysis of Affinity Separations. I: Predicting the Performance of Affinity Adsorbers," *Chem. Eng. J.*, **30**, B9 (1985).

Arve, B. H., and A. I. Liapis, "Biospecific Adsorption in Fixed and Periodic Countercurrent Beds," *Biotechnol. Bioeng*., **32**, 616 (1988).
Bautista, L. F., M. Martínez, and J. Aracil, "Adsorption Equilibrium of α-Amylase in Aqueous Solutions," *AIChE J*., **45**(4), 761 (1999).
Bautista, L. F., M. Martínez, and J. Aracil, "Modelling of the Adsorption of α-Amylase in Batch Stirred Tank," *Ind. Eng. Chem. Res*., **39**(11), 4320 (2000).
Boel, E., L. Bradi, A. M. Brzozowski, Z. S. Derewenda, G. G. Dodson, V. J. Jensen, S. B. Petersen, H. Swift, L. Thim, and H. F. Woldike, "Calcium Binding in Alpha-Amylases: An X-Ray Diffraction Study at 2.1 Å Resolution of Two Enzymes from *Aspergillus*," *Biochemistry*, **29**(26), 6244 (1990).
Carberry, J. J. "A Boundary-Layer Model of Fluid-Particle Mass Transfer in Fixed Beds," *AIChE J*., **6**(3), 460 (1960).
Carey, G. F., and B. A. Finlayson, "Orthogonal Collocation of Finite Elements," *Chem. Eng. Sci*., **30**, 587 (1975).
Carta, G., and R. K. Lewus, "Film Model Approximation for Multicomponent Adsorption," *Adsorption*, **6**, 5 (2000).
Chase, H. A., "Prediction of the Performance of Preparative Affinity Chromatography," *J. Chromatogr*., **297**, 179 (1984).
Danckwerts, P. V., "Continuous Flow Systems. Distribution of Residence Time," *Chem. Eng. Sci*., **2**, 1 (1953).
Gear, C. W., *Numerical Initial Value Problems in Ordinary Differential Equations*, Prentice-Hall, Englewood Cliffs, NJ (1971).
Hidajat, K., J. Aracil, J. J. Carberry, and C. N. Kenney, "Interphase Fluid-Particle Mass Transport at Low Reynolds Numbers," *Catal. Lett*., **30**, 213 (1995).
Hougen, O. A., "Engineering Aspects of Solid Catalysts," *Ind. Eng. Chem*., **53**(7), 509 (1961).
Hsiung, T. H., and G. Thodos, "Mass Transfer Factor from Actual Driving Forces for the Flow of Gases Through Packed Beds ($0.1 < Re < 100$)" *Int. J. Heat Mass Transfer*., **20**(4), 331 (1977).
Janecek, S., and S. Baláž, "Alpha-Amylases and Approaches Leading to their Enhanced Stability," *FEBS Lett*., **304**(1), 1 (1992).
Johnston, A., Q. M. Mao, and M. T. W. Hearn, "Analysis of Operating Parameters Affecting the Breakthrough Curves in Fixed-Bed Chromatography of Proteins Using Several Mathematical Models," *J. Chromatogr*., **548**, 127 (1991).
Mao, Q. M., and M. T. W. Hearn, "Optimization of Affinity and Ion Exchange Chromatographic Processes for the Purification of Proteins," *Biotechnol. Bioeng*., **52**, 204 (1996).
Miyabe, K., and G. Guiochon, "Kinetic Study of the Concentration Dependence of the Mass Transfer Rate in Anion-Exchange Chromatography of Bovine Serum Albumin," *Biotechnol. Progr*., **15**(4), 740 (1999).
Niemeyer, B., T. Feilenreiter, and H. Tiltscher, "Theoretical Studies on Biospecific Adsorption for Large-Scale Affinity Separations," *Chem. Eng. Sci*., **51**(24), 5263 (1996).
Polson, A., "Some Aspects of Diffusion in Solution and a Definition of a Colloidal Particle," *J. Phys. Colloid Chem*., **54**, 649 (1950).
Sajonz, P., H. Guan-Sajonz, G. Zhong, and G. Guiochon, "Application of the Shock Layer Theory to the Determination of the Mass-Transfer Rate Coefficient and Its Concentration Dependence for Proteins on Anion Exchange Columns," *Biotechnol. Progr*., **13**(2), 170 (1997).
Skidmore, G. L., B. J. Horstman, and H. A. Chase, "Modelling Single-Component Protein Adsorption to the Cation Exchanger S Sepharose FF," *J. Chromatogr*., **498**, 113 (1990).
Sridhar, P., "Modelling of Affinity Separation by Batch and Fixed Bed Adsorption—A Comparative Study," *Chem. Eng. Technol*., **19**, 357 (1996).
Sridhar, P., N. V. S. Sastri, J. M. Modak, and A. K. Mukherjee, "Mathematical Simulation of Bioseparation in an Affinity Packed Column," *Chem. Eng. Technol*., **17**, 422 (1994).
Swift, H. J., L. Brady, Z. S. Derewenda, E. Dodson, G. G. Dodson, J. P. Turkenburg, and A. Wilkinson, "Structure and Molecular Model Refinement of *Aspergillus oryzae* (TAKA) Alpha-Amylase: An Application of the Simulated-Annealing Method," *Acta Crystall*., **B47**, 535 (1991).
Vallee, B. L., E. A. Stein, W. N. Sumerwell, and E. H. Fischer, "Metal Content of Alpha-Amylase of Various Origins," *J. Biol. Chem*., **234**(11), 2901 (1959).
Villadsen, J. V., and W. E. Stewart, "Solution of Boundary-Value Problems by Orthogonal Collocation," *Chem. Eng. Sci*., **22**, 1483 (1967).
Wankat, P. C., *Rate-Controlled Separations*, Blackie, Glasgow (1994).
Yang, H., M. Bitzer, and M. R. Etzel, "Analysis of Protein Purification Using Ion-Exchange Membranes," *Ind. Eng. Chem. Res*., **38**, 4044 (1999).

Manuscript received Sept. 30, 2002, and revision received Mar. 4, 2003.